

# Coordinating Biointeraction and Bioreaction of a Nanocarrier Material and an Anticancer Drug to Overcome Membrane Rigidity and Target Mitochondria in Multidrug-Resistant Cancer Cells

Rui Xue Zhang, Lily Yi Li, Jason Li, Zhensong Xu, Azhar Z. Abbasi, Lucy Lin, Mohammad A. Amini, Wei Yu Weng, Yu Sun, Andrew M. Rauth, and Xiao Yu Wu\*

Multidrug resistance (MDR) is a main cause of chemotherapy failure in cancer treatment. It is associated with complex cellular and molecular mechanisms including overexpression of drug efflux transporters, increased membrane rigidity, and impaired apoptosis. Numerous efforts have been made to overcome efflux transporter-mediated MDR using nanotechnology-based approaches. However, these approaches fail to surmount plasma membrane rigidity that attenuates drug penetration and nanoparticle endocytosis. Here, a “one-two punch” nanoparticle approach is proposed to coordinate intracellular biointeraction and bioreaction of a nanocarrier material docosahexaenoic acid (DHA) and an anticancer prodrug mitomycin C (MMC) to enhance mitochondrion-targeted toxicity. Incorporation of DHA in solid polymer-lipid nanoparticles first reduces the membrane rigidity in live cancer cells thereby increasing nanoparticle cellular uptake and MMC accumulation. Subsequent intracellular MMC bioreduction produces free radicals that in turn react with adjacent DHA inducing significantly elevated mitochondrial lipid peroxidation, leading to irreversible damage to mitochondria. Preferential tumor accumulation of the nanoparticles and the synergistic anticancer cytotoxicity remarkably inhibit tumor growth and prolonged host survival without any systemic toxicity in an orthotopic MDR breast tumor model. This work suggests that combinatorial use of biophysical and biochemical properties of nanocarrier materials with bioactive prodrugs is a powerful approach to overcoming multifactorial MDR in cancer.

## 1. Introduction

Chemotherapy is a primary treatment modality for metastatic cancer. However, the development of multidrug resistance (MDR) in cancer leads to treatment failure in the clinic.<sup>[1]</sup> MDR is associated with multifactorial cellular and molecular mechanisms, including overexpression of efflux transporters (e.g., P-glycoprotein (*P-gp*)), increased membrane rigidity, and impaired apoptosis.<sup>[2]</sup> Mitochondria, as subcellular organelles, play a critical role in driving drug-resistance through elevated oxidative stress and mitochondrial DNA mutation.<sup>[3]</sup> Thus, to exploit mitochondrial targets, various mitochondria-targeted drugs (e.g., prodrugs, mitochondrial peptides) and mitochondriotropics have been investigated.<sup>[3c,4]</sup> However, MDR cancer cells exhibit multiple barriers to drug uptake,<sup>[5]</sup> among which overexpression of *P-gp* efflux transporters and rigidity of the plasma membrane present the first cellular barrier to drug delivery, preventing mitochondrial drugs from entry into many types of MDR cancer cells.<sup>[3c,5,6]</sup>

Dr. R. X. Zhang, L. Y. Li, Dr. J. Li, Dr. A. Z. Abbasi, L. Lin, M. A. Amini, Prof. X. Y. Wu  
Advanced Pharmaceuticals and Drug Delivery Laboratory  
Leslie Dan Faculty of Pharmacy  
University of Toronto  
144 College Street, Ontario M5S 3M2, Canada  
E-mail: xywu@phm.utoronto.ca  
Z. Xu, Prof. Dr. Y. Sun  
Advanced Micro and Nanosystems Laboratory  
Department of Mechanical and Industrial Engineering  
University of Toronto  
5 King's College Road, Toronto, Ontario M5S 3G8, Canada

Prof. W. Y. Weng  
School of Pharmacy  
East China University of Science and Technology  
130 Meilong Road, Shanghai 200237, China  
Prof. A. M. Rauth  
Departments of Medical Biophysics and Radiation Oncology  
University of Toronto  
Princess Margaret Cancer Centre  
610 University Avenue, Toronto, Ontario M5G 2M9, Canada

 The ORCID identification number(s) for the author(s) of this article can be found under <https://doi.org/10.1002/adfm.201700804>.

DOI: 10.1002/adfm.201700804

Various approaches have been attempted to overcome membrane drug efflux transporters in MDR cancers, such as application of *P-gp* inhibitors. The combination of *P-gp* inhibitors with chemotherapy has been studied in clinical trials, but did not generate positive results partially due to the nonoptimal spatiotemporal biodistribution of *P-gp* inhibitors and anticancer drugs in the body.<sup>[7]</sup> Nanoparticles have shown an ability to bypass efflux transporters (e.g., *P-gp*) and deliver various types of anticancer drugs with or without *P-gp* modulators against MDR cells.<sup>[8]</sup> However, the alteration of membrane composition and rigidity in *P-gp* overexpressing MDR cells impairs nanoparticle endocytosis, a primary entry pathway for nanoparticles and some anticancer drugs, hindering drug uptake and anticancer efficacy.<sup>[2b,6,9]</sup> This phenomenon has been demonstrated by recent biophysical studies of extracted plasma membrane from MDR cancer cells, in which *P-gp* overexpressing cytoplasmic membrane shows high amounts of cholesterol and sphingolipids.<sup>[2b,9a,b,10]</sup> These lipids tend to form lipid rafts that co-exist with the transporter proteins, complementing the transporters and supporting their efflux function.<sup>[2b,9b]</sup> Such lipid rafts in MDR cell membrane are insoluble in commonly used membrane detergents; thus application of the detergents does not improve cellular nanoparticle uptake.<sup>[9a,11]</sup> Although the biophysical properties of lipid rafts in MDR cell membranes have been investigated,<sup>[12]</sup> a drug delivery approach to overcoming lipid rafts-associated MDR is still lacking. Only a limited number of studies have sought to overcome membrane-rigidity of MDR cancer cells. They involve pretreatment with epigenetic drugs to change membrane lipid compositions or nanoparticle interactions to biomechanically bend the plasma membrane.<sup>[13]</sup> Yet, the complexity of MDR in cancer requires multifunctional drug delivery approaches. Herein we have designed a nanocarrier system to surmount multiple drug barriers in MDR cancer cells and target organelles responsible for molecularly driven drug-resistance (e.g., mitochondria) by utilizing the intracellular synergistic biointeraction and bioreaction between a nanocarrier material and an anticancer prodrug.

The poly-unsaturated fatty acid docosahexaenoic acid (DHA), a naturally occurring liquid lipid, has been used as a nanocarrier material incorporated in solid lipid matrix nanoparticles to enhance particle stability and drug loading.<sup>[14]</sup> DHA has also been integrated into phospholipid-containing plasma membranes to enhance bending.<sup>[15]</sup> The presence of multiple carbon-carbon double bonds (C=C) in free DHA makes it prone to nonenzymatic lipid peroxidation by exogenous reactive oxygen species (ROS) produced by some anticancer drugs, resulting in enhanced chemosensitivity in various cancer cell types.<sup>[16]</sup> Inspired by both the biophysical and biochemical properties of DHA, herein a novel mitomycin C (MMC)-loaded, DHA-containing solid polymer-lipid nanoparticle (PLN) system was designed to sequentially target membrane rigidity and mitochondria in MDR breast cancer cells, i.e., a “two-step” strategy to tackle multifaceted MDR (Figure 1a). MMC is a potent alkylating prodrug that undergoes intracellular bioreduction by a 2-electron reductase in the cytosol (e.g., DT-diaphorase) and 1-electron reductases in mitochondria (e.g., cytochrome b5 reductase) (Figure 1b).<sup>[17]</sup> Exogenous ROS produced by intramitochondrial bioreduction of MMC then attacks DHA triggering a lipid peroxidation chain reaction at mitochondrial sites

(Figure 1b).<sup>[17]</sup> We hypothesize that the DHA-incorporated PLN with loaded MMC (MMC-DHA-PLN) can intracellularly coordinate biointeraction and bioreaction of DHA and MMC leading to enhanced anticancer effects in MDR cancer cells.

## 2. Results and Discussion

### 2.1. Rational Selection of Mono- versus Poly-Unsaturated Liquid Lipids for Formulating PLN

Prior to making the PLN system, we carefully reviewed properties of unsaturated liquid lipids<sup>[5,18]</sup> and identified two candidates of unsaturated fatty acids (FA), i.e., a mono-unsaturated FA oleic acid (OA) and a poly-unsaturated fatty acid DHA. Incorporation of low melting temperature FA (i.e., OA or DHA) into PLN could spatially create amorphous form within its solid lipid matrix, thus improving drug loading, colloidal stability and reducing initial burst drug release.<sup>[5,14,19]</sup> Our previous study of mono-unsaturated OA (unpublished data) showed that PLN made of binary mixtures of OA and a solid lipid improved physicochemical stability and increased encapsulation of a hydrophilic drug (i.e., doxorubicin) via ionic interactions compared to PLN composed only of solid lipids.<sup>[20]</sup> To rationally design a desired PLN system for the cancer cells of interest (i.e., murine MDR EMT6/AR1 breast cancer cells), an investigation of the synergistic anticancer effect of FA and MMC was performed. The dose-response curves of OA or DHA alone as well as in combination with MMC were measured and the possible synergism of the interaction was analyzed by the median effect analysis.<sup>[21]</sup> Both DHA alone and DHA-MMC were more potent than OA and OA-MMC against MDR EMT6/AR1 cells (Figure 2a). Free DHA-MMC exhibited a strong anticancer synergism with a combination index (CI) less than 1 in both MDR EMT6/AR1 (Figure 2b) and drug-sensitive EMT6/WT cancer cells (Figures S1 and S2, Supporting Information). In contrast, free OA-MMC showed an antagonism at the studied doses with CI greater than 1 (Figure 2b). The higher anticancer potency and synergy of DHA-MMC may be ascribed to a larger number of unsaturated C=C bonds in DHA than OA, imparting higher bioreactivity of DHA vital to mitochondrion-targeted lipid peroxidation.<sup>[22]</sup> Based on these screening results, DHA was selected as the liquid lipid component of PLN at a synergistic molar ratio of DHA:MMC = 0.6:1, which was identified in our preliminary work, to make MMC-loaded PLN for further studies.

### 2.2. Particle Properties of Various PLN Formulations

Various PLN formulations were prepared by sequential two-step sonication followed by a self-assembly process using the formulation compositions presented in Table S1 of the Supporting Information.<sup>[5]</sup> The particle properties (Figure 3a, Figure S3, Supporting Information) indicate that these PLNs are suitable for intravenous (i.v.) administration with average diameters ranging from 71 to 96 nm and negative surface charges from -36 to -57 mV. Spherical MMC-DHA-PLN with an average diameter of ≈88 nm and polydispersity index

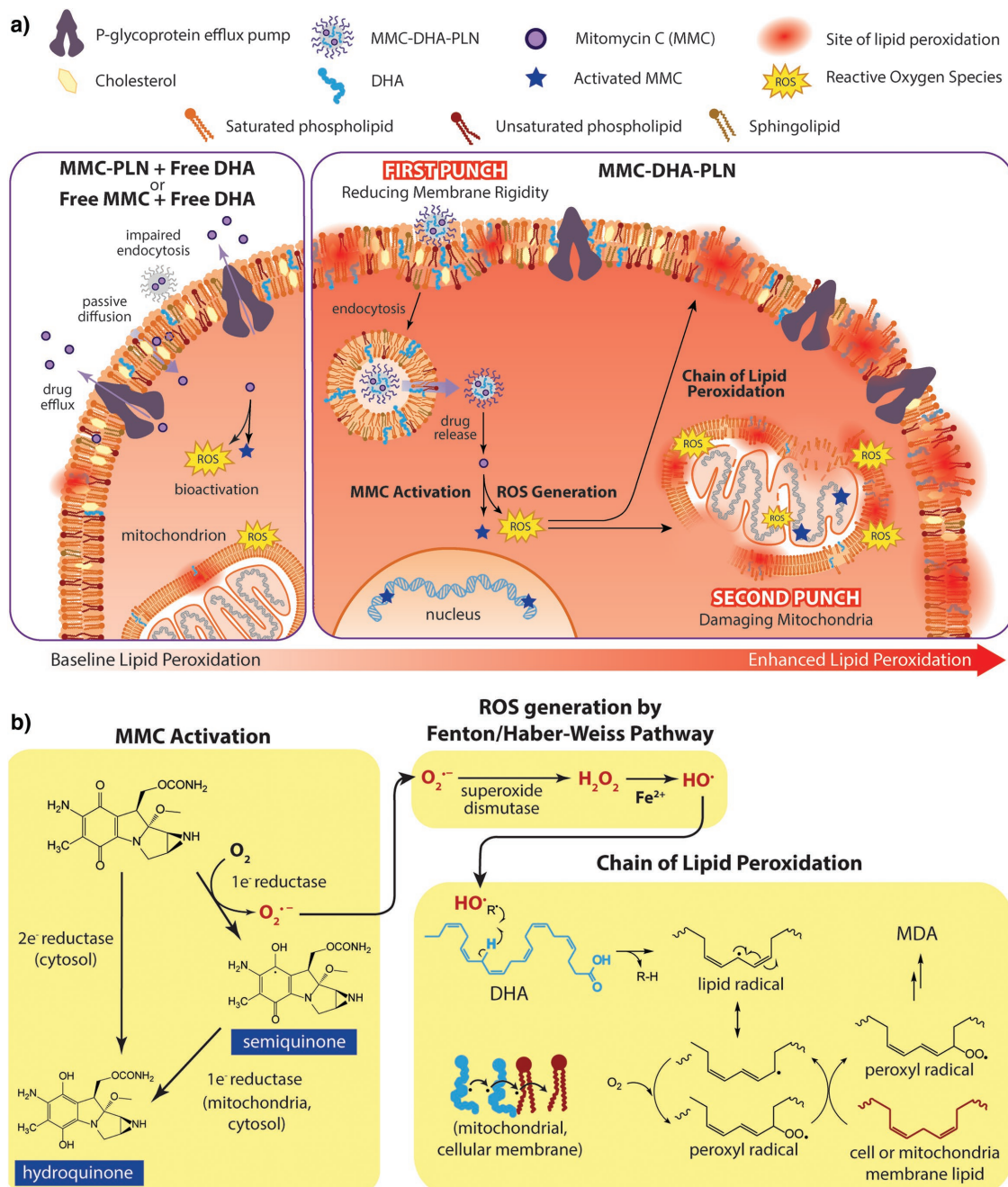


**Figure 1.** Illustration of one-two punch (two-step) strategy that coordinates poly-unsaturated fatty acid DHA and ROS generating prodrug MMC within a single PLN system for intracellular targeted mitochondrial lipid peroxidation in MDR cancer cells. a) Left panel: the rigid cytoplasmic membrane of MDR cancer cells prevents both nanoparticles (e.g., MMC-PLN) and free drug (e.g., free MMC) from entry and accumulation within cells. Free drug could be trapped within the thickened plasma membrane and pumped out by *P-gp* efflux transporters, while nanoparticles cannot enter cells due to impaired endocytosis. Co-treatment with free DHA does not appreciably improve the cellular uptake of nanoparticles and free drug; right panel: one-two punch strategy of using MMC-DHA co-loaded PLN (MMC-DHA-PLN). First, MMC-DHA-PLN reduces plasma membrane rigidity thus enhancing cellular PLN uptake; second, MMC bioactivation by mitochondria enzymes (e.g., cytochrome b5 reductase) generates ROS that cause peroxidation of DHA in MMC-DHA-PLN, leading to oxidative damage of mitochondria and possibly plasma membranes. b) Biochemical pathways of MMC activation and lipid peroxidation. The subcellular delivery of prodrug MMC is bioactivated by two-electron reductases in cytosol and one-electron reductases in mitochondria. Superoxide (O<sub>2</sub><sup>-</sup>) generated during MMC one-electron reduction can enter the Fenton/Haber-Weiss pathway to generate hydroxyl radicals (OH<sup>•</sup>) that in turn attack the methylene bridge between C=C double bonds of DHA to initiate a chain of lipid peroxidation, resulting in elevated oxidative damage to mitochondria and possibly cell membranes.

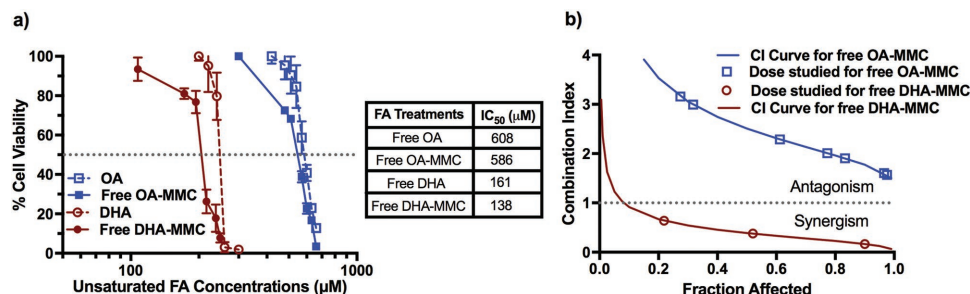


**Figure 2.** Screening mono- or poly-unsaturated FA as a bioreactive nanomaterial of PLN for treating MDR EMT6/AR1 cancer cells. a) Dose-response curves of free OA or DHA as well as their combination with the anticancer prodrug MMC and table of resultant  $\text{IC}_{50}$ . b) CI curves of free OA-MMC and free DHA-MMC. The molar ratio of 0.6:1 for free DHA-MMC and 1.4:1 for free OA-MMC were used to evaluate their synergistic interactions. CI > 1 and CI < 1 indicate antagonism and synergism, respectively. Results are expressed as mean  $\pm$  standard error of the mean (SEM) ( $n = 3$ ).

(PDI)  $\approx 0.2$  were obtained (Figure 3a). A stronger electronegative  $\zeta$ -potential of MMC-DHA-PLN ( $-43.7$  mV) compared to MMC-PLN ( $-35.7$  mV) may arise from the presence of an anionic form of DHA potentially present at the interface of PLN. Above 90% MMC encapsulation efficiency was achieved in MMC-DHA-PLN which was threefold higher than our previous PLN formulation without DHA.<sup>[23]</sup> MMC-DHA-PLN in serum showed unchanging particle size and turbidity as measured by transmittance (Figure 3d,e), suggesting good colloidal stability for in vivo use. The size,  $\zeta$ -potential and PDI of MMC-

DHA-PLN stored at  $4^\circ\text{C}$  also remained unchanged over 28 d (Figure 3f). Biphasic release of MMC from MMC-DHA-PLN was observed in which 20% of MMC was released in the first 4 h followed by a sustained slow release of MMC up to almost 60% at 96 h (Figure 3g). From the therapeutic point of view, the fast drug release from PLN enables cancer cell exposure to the bioavailable drug following i.v. injection of the nanoparticle formulation. On the other hand, sustained drug release is preferred during systemic circulation of PLN before reaching the tumor site to minimize unnecessary normal tissue toxicity.<sup>[5,8a,b]</sup>

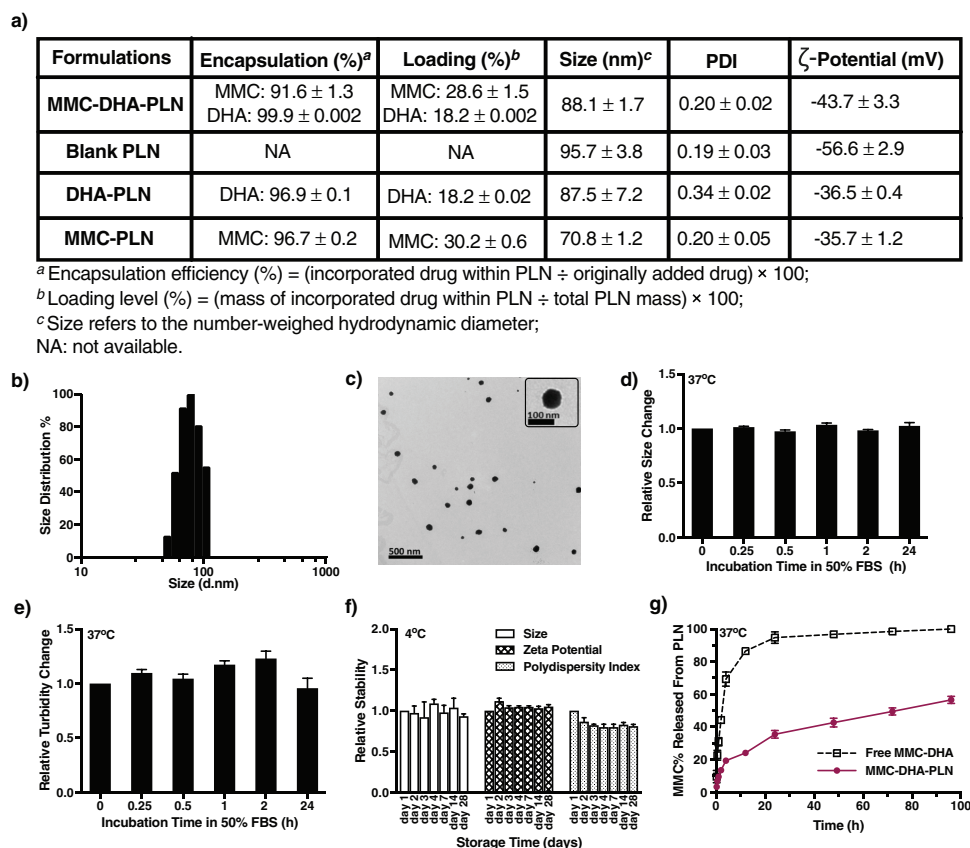


**Figure 3.** Characterization of MMC-DHA-PLN. a) Comparison of physical parameters among various PLN formulations. b) Dynamic light scattering (DLS) size distribution. c) Transmission electron microscopy (TEM) shows spherical morphology. d,e) Serum stability in 50% FBS at  $37^\circ\text{C}$  over 24 h. f) Storage stability at  $4^\circ\text{C}$  over 28 d. g) MMC release profiles at  $37^\circ\text{C}$  in 10% FBS over 96 h. Data are given as mean  $\pm$  SEM with  $n = 3$ .

The in vitro drug release assay may not completely reflect what happens in vivo due to the impact of complicated biological systems (e.g., blood protein binding, tumor tissue) on drug release kinetics. However, based on our previous pharmacokinetic studies of PLN<sup>[8b]</sup> the sustained drug release profile of MMC-DHA-PLN should provide sufficient drug within tumor tissue and cancer cells for an anticancer effect.

### 2.3. Biointeraction of DHA Reduces Membrane Rigidity and Enhances Intracellular PLN and Drug Uptake

The *P-gp* overexpressing MDR EMT6/AR1 murine breast cancer cells<sup>[24]</sup> were used in all studies, with its parent drug-sensitive EMT6/WT cells for comparison (Figures S4 and S5, Supporting Information). To investigate “the first step” of MMC-DHA-PLN to overcome membrane-rigidity associated barrier to drug delivery, the membrane rigidity of the cell lines was characterized using atomic force microscopy (AFM) (Figure S6, Supporting Information). Compared to EMT6/WT cells, the cytoplasmic membrane of EMT6/AR1 cells exhibited significantly higher rigidity, as indicated by a higher Young’s modulus (Figure 4a). In vitro treatment with free DHA alone, or in combination with free MMC, or with MMC-DHA-PLN significantly reduced membrane rigidity of EMT6/AR1 cells (Figure 4b). Despite the effect of DHA-containing treatments on reducing membrane rigidity, no significant enhancement on drug accumulation was observed in cells treated with free MMC-DHA at 4 h (Figure 4c), likely due to free MMC trapped within the thick membrane and pumped out by *P-gp*.<sup>[2b,9b]</sup> In contrast, intracellular MMC accumulation was increased by eightfold after treatment with MMC-DHA-PLN compared to MMC-PLN, suggesting the role of DHA as a nanomaterial in facilitating drug accumulation in MDR cancer cells.

We next investigated whether co-localization of DHA with PLN is critical for enhanced cellular uptake of PLN by treating EMT6/AR1 cells with four different types of PLN labeled with the lipophilic fluorescent dye, Nile red (NR). The  $\zeta$ -potential of PLN appeared to vary with formulations (Figure 3a) which could potentially influence their cellular internalization.<sup>[25]</sup> However, fluorescence microscopy examination revealed that PLN accumulation (red dots) throughout the cytoplasm and clustered around nuclei was only observed in MMC-DHA-PLN (NR) treated MDR cells (Figure 4d). In contrast, MMC-PLN (NR) with less negative surface charge (−35.7 mV) than MMC-DHA-PLN (−43.7 mV) did not appreciably improve the PLN uptake compared to blank PLN (NR) and even with co-treatment with free DHA (Figure 4d). This observation suggests that co-encapsulation of DHA with MMC in PLN is more pivotal in facilitating cellular uptake of PLN by the MDR EMT6/AR1 cells than the  $\zeta$ -potential difference in various PLN formulations. Quantitative analysis using flow cytometry further showed that the cells treated with MMC-DHA-PLN (NR) exhibited nearly threefold higher intracellular fluorescence intensity than other treatment groups after 4 h exposure at an equivalent dose (Figure 4e,f). The cellular uptake of MMC-DHA-PLN was evident at 37 °C, but not at 4 °C, suggesting an energy-dependent endocytotic process rather than passive accumulation of nanoparticles (Figure 4e,f).<sup>[26]</sup>

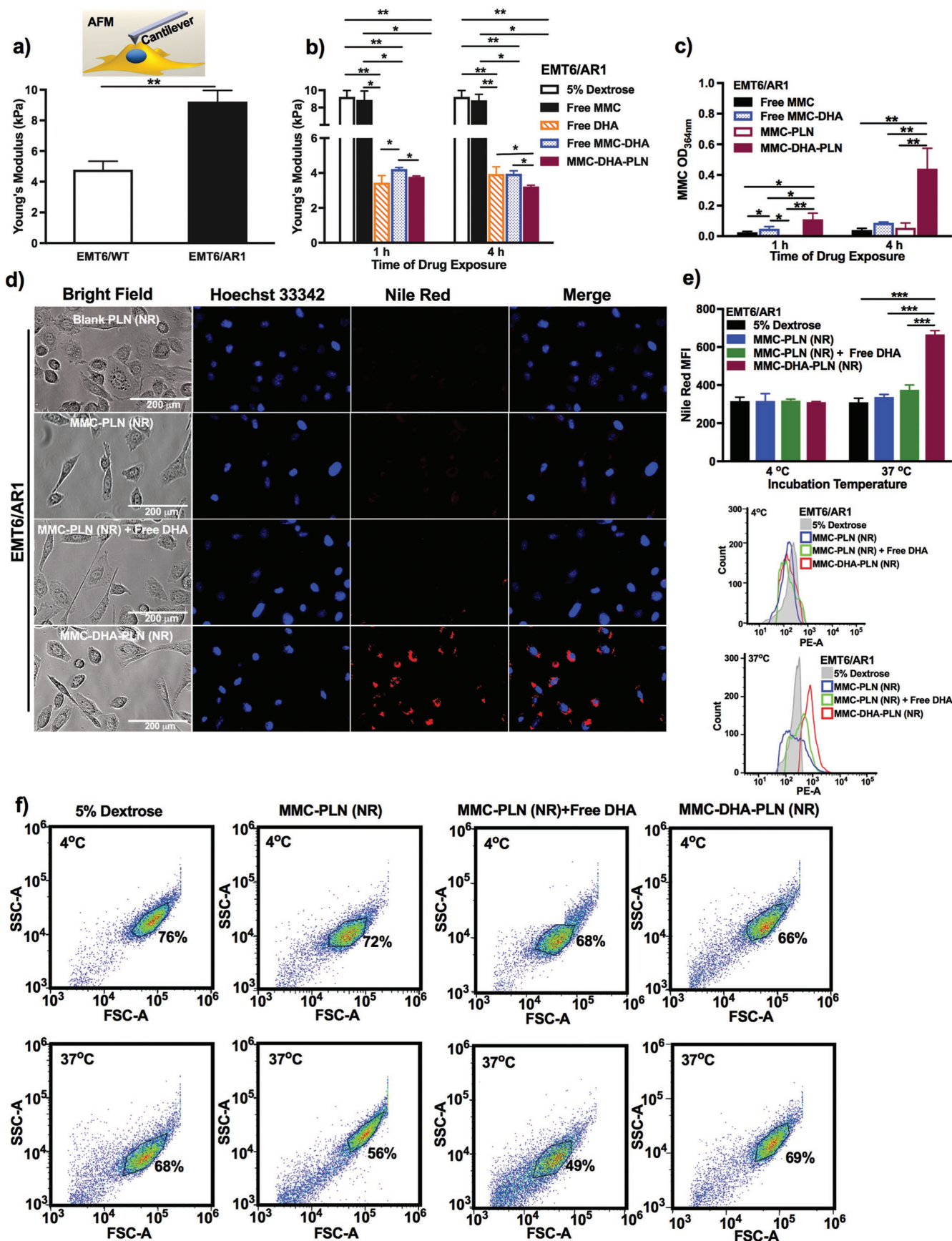
### 2.4. Intracellular Bioreaction between MMC and DHA Elevates Mitochondrion-Targeted Lipid Oxidation

To study the effect of MMC-DHA-PLN on mitochondrion-targeted lipid peroxidation in MDR EMT6/AR1 cells, a natural by-product of lipid peroxidation, malondialdehyde (MDA), was measured following various treatments at 4 and 24 h. Significantly enhanced lipid peroxidation was seen as early as 4 h in MMC-DHA-PLN-treated cells as compared to monotherapies (i.e., free MMC, free DHA) which showed no effect on MDA levels, while free MMC-DHA only modestly increased lipid peroxidation at 24 h (Figure 5a). This result suggests the importance of intracellular bioreactions between MMC-produced ROS and DHA especially in a coordinated way through the same nanocarrier. Consistent with continuously elevated lipid peroxidation, MMC-DHA-PLN treated MDR cancer cells showed profoundly damaged mitochondria (i.e., altered ultrastructural morphology), the degree of which increased with treatment time from 4 to 24 h as evidenced by TEM photographs (Figure 5b). In contrast, the cells treated with 5% dextrose displayed uniform cytosol and evenly distributed intact mitochondria (Figure 5b).

To further confirm that elevated lipid peroxidation induced by MMC-DHA-PLN occurred at mitochondrial sites, laser scanning confocal fluorescence microscopy was applied. In MMC-DHA-PLN treated cells, the fluorescent dye (BODIPY581/591) shifted from red (reduced state) to a strong green fluorescence (oxidized state) in the cytoplasm 4 h post-treatment, indicating substantial lipid peroxidation, compared to cells treated with 5% dextrose which only showed red fluorescence with sparse green dots (Figure 5c). Quantitative analysis of the fluorescence ratio (green/red) also revealed a nearly threefold higher baseline lipid peroxidation in untreated EMT6/AR1 cells compared to parent drug-sensitive EMT6/WT cells (Figure 5d), indicating excessive ROS generation in MDR cancer cells that could be a target for lipid-oxidation therapy.<sup>[10a]</sup> To identify the subcellular site of lipid peroxidation, mitochondria of cancer cells were stained with Mitotracker Deep Red. In MMC-DHA-PLN treated cells, strong green fluorescence of lipid peroxidation was visualized to co-localize with far-red fluorescence of mitochondria (Figure 5e, Figure S5, Supporting Information). Pearson’s correlation coefficient (PCC)<sup>[27]</sup> of co-localized images was found to be 0.69 and 0.54 for MDR EMT6/AR1 and drug-sensitive EMT6/WT cells, respectively (Figure 5f), which indicates a positive correlation between green (lipid peroxidation) and red (mitochondria) pixels, supporting the hypothesis of mitochondrion-targeted lipid-oxidation.

### 2.5. MMC-DHA-PLN Enhances Anticancer Efficacy In Vitro and In Vivo

Finally, the “two-step” strategy using MMC-DHA-PLN was evaluated at the anticancer efficacy level in MDR cancer cells both in vitro and in vivo. The cytotoxicity of various treatments as a function of drug doses was determined by the 3-(4,5-dimethylthiazol-2-yl)-2,5-diphenyl tetrazolium bromide (MTT) assay. The MMC concentration of MMC-DHA-PLN to reduce the viability of 50% MDR EMT6/AR1 cancer cells



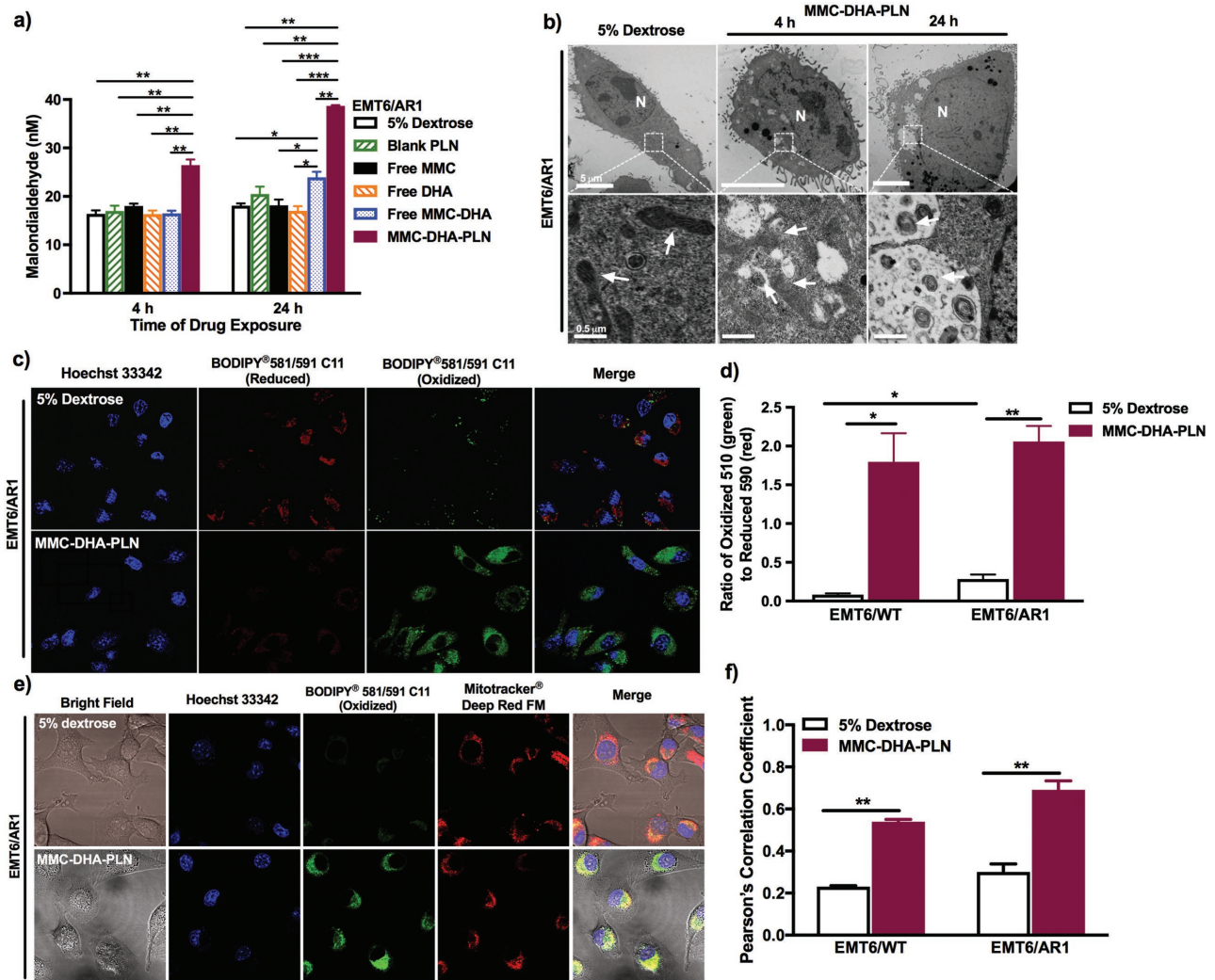


**Figure 5.** MMC-DHA-PLN targeted mitochondrial lipid peroxidation in MDR EMT6/AR1 breast cancer cells. a) The level of MDA before and after various free MMC and/or DHA formulations, blank PLN or MMC-DHA-PLN for 4 or 24 h. b) TEM images of drug-resistant cells treated with 5% dextrose and MMC-DHA-PLN for 4 and 24 h. The nondamaged mitochondria for 5% dextrose and damaged mitochondria for MMC-DHA-PLN treatment groups are indicated with white arrows and N represents nucleus. c) Laser scanning confocal microscope images (60 $\times$ ) of lipid peroxidation in living EMT6/AR1 cells treated with 5% dextrose or MMC-DHA-PLN. d) Quantitative analysis of lipid peroxidation in both drug-sensitive EMT6/WT and MDR EMT6/AR cells by calculating the ratio of fluorescence intensity using fluorescein isothiocyanate (FITC) channel at 510 nm and Texas Red channel at 590 nm. e) Laser scanning confocal microscope images (60 $\times$ ) of lipid peroxidation localization (green fluorescence using FITC channel) in mitochondria (red fluorescence using Alexa Fluor 647 channel) of cells treated with 5% dextrose or MMC-DHA-PLN. f) Degree of colocalization between lipid peroxidation and mitochondria determined by PCC in both EMT6/WT and EMT6/AR1 cells. The results are expressed as mean  $\pm$  SEM with  $n = 3-4$  (\* $p < 0.05$ , \*\* $p < 0.01$ , and \*\*\* $p < 0.001$ ). All cancer cells were treated with  $24 \times 10^{-6}$  M of MMC or  $14 \times 10^{-6}$  M of DHA or the combination of MMC-DHA.

**Figure 4.** (previous page) MMC-DHA-PLN overcomes membrane rigidity to enhance intracellular PLN uptake and drug accumulation in MDR EMT6/AR1 breast cancer cells. a) Comparison of Young's modulus of drug-sensitive EMT6/WT and MDR EMT6/AR1 breast cancer cells using AFM (schematic of technique). b) Young's modulus of EMT6/AR1 cells after treatment with 5% dextrose or MMC and/or DHA in free or PLN formulations for 1 and 4 h. c) Effect of DHA in free or PLN formulation on intracellular MMC accumulation. d) Intracellular localization of blank PLN (NR), MMC-PLN (NR), MMC-PLN (NR) + Free DHA and MMC-DHA-PLN (NR). Fluorescence images (20 $\times$ ) were acquired after 4 h treatment at the concentrations of  $105 \times 10^{-6}$  M of NR. e) Flow cytometry quantitation of intracellular PLN uptake by analyzing NR fluorescence intensity for 5% dextrose, MMC-PLN (NR), MMC-PLN (NR) + Free DHA, or MMC-DHA-PLN (NR) after 4 h treatment at 4  $^{\circ}$ C and 37  $^{\circ}$ C. f) Representative examples of the dot plots for differentiating uniform and normal cell population from cell debris or damaged cells. Forward-scattered light (FSC, x-axis) and side-scattered light (SCC, y-axis) measures cell surface areas and cell granularity, respectively. Total  $1 \times 10^4$  cells were selected and only normal and uniform cells were chosen for intensity analysis (circled with blue line and percent of cell numbers). Results are expressed as mean  $\pm$  SEM with  $n = 3$  (\* $p < 0.05$ , \*\* $p < 0.01$ , and \*\*\* $p < 0.001$ ). All cancer cells were treated with  $24 \times 10^{-6}$  M of MMC or  $14 \times 10^{-6}$  M of DHA or the combination MMC and DHA.

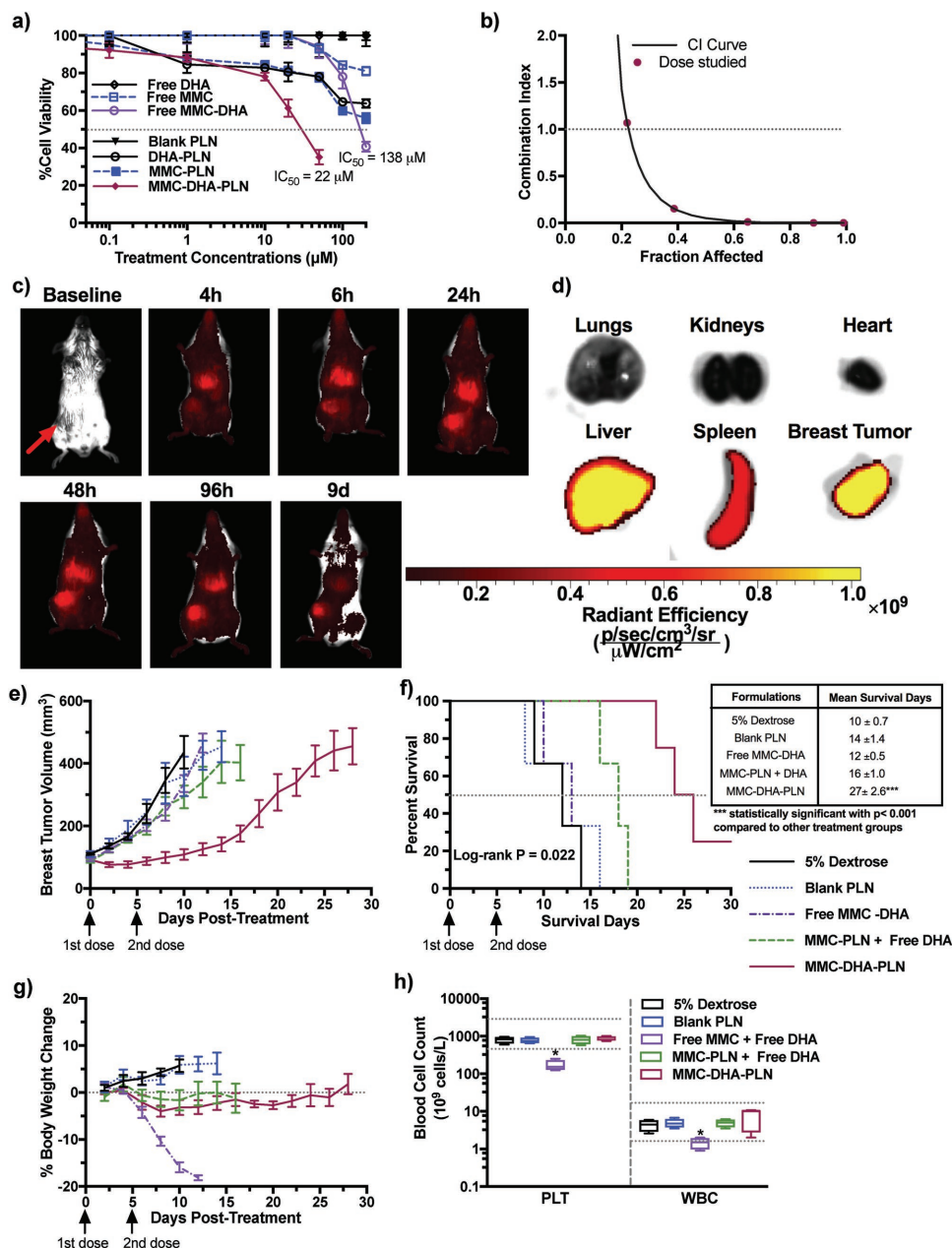


**Figure 6.** Synergistic anticancer therapy of MMC-DHA-PLN in MDR EMT6/AR1 cancer cells and tumors. a) Cytotoxicity of MMC and/or DHA in free or PLN formulations. Data for free MMC-DHA and MMC-DHA-PLN plotted on the basis of the MMC concentrations ranging from  $0.01 \times 10^{-6}$  to  $200 \times 10^{-6}$  M and cytotoxicity was assessed by an MTT cell viability assay after 24 h exposure to various treatment groups.  $\text{IC}_{50}$  of MMC-DHA-PLN to kill 50% MDR cancer cells was  $22 \times 10^{-6}$  M as compared to  $138 \times 10^{-6}$  M of free MMC-DHA. b) Anticancer synergism (CI < 1) of MMC-DHA-PLN determined by median effect analysis. c) In vivo biodistribution of MMC-DHA-PLN (DiR). d) Ex vivo organ biodistribution of MMC-DHA-PLN (DiR) at 48 h post-treatment. e) EMT6/AR1 breast tumor growth over 30 d after two sequential dose regimens. f) Kaplan–Meyer survival curves of MMC-DHA combination in free or PLN formulations. g) Body weight change over 30 d post-treatment. h) PLT and WBC count for myelosuppression caused by MMC involved treatments. All mice were i.v. injected on day 0 and day 5 with  $4.0 \text{ mg kg}^{-1}$  of MMC and  $2.4 \text{ mg kg}^{-1}$  of DHA according to the predetermined synergistic 1:0.6 molar ratio of MMC and DHA combination. Data points represent the mean  $\pm$  SEM with  $n = 5\text{--}6$  mice for each treatment ( $*p < 0.05$ ,  $**p < 0.01$ , and  $***p < 0.001$ ).

( $\text{IC}_{50} = 22 \times 10^{-6}$  M) was about one-sixth that of free MMC-DHA ( $\text{IC}_{50} = 138 \times 10^{-6}$  M) (Figure 5a), while DHA alone was non-toxic at studied doses below  $200 \times 10^{-6}$  M (Figure 5a). These results indicate both reduction in cell number and mitochondrial dysfunction after treatments since the MTT assay measures reduction in the formation of formazan from tetrazole

using mitochondrial enzymes.<sup>[28]</sup> Consistent with the mechanistic studies in which continuously elevated lipid peroxidation and increased severity of mitochondrial damage were observed from 4 to 24 h (Figure 5a,b), 24 h treatment of MDR cancer cells with MMC-DHA-PLN reduced cell viability by more than 50% (Figure 6a). It is worth noting that cytotoxicity of

MMC-DHA-PLN against MDR cancer cells was likely caused by the dual-action of MMC induced DNA crosslinking<sup>[17b]</sup> and oxidative damage of mitochondria (Figure 1a). The observed larger effect on reducing cell viability of MMC-DHA-PLN than monotherapy (i.e., free MMC, MMC-PLN) (Figure 6a) suggests a pivotal role of the nanomaterial DHA in the nanoparticle mediated lipid-peroxidation therapy against MDR cancer cells. The anti-cancer synergism of MMC-DHA-PLN, evidenced by a CI less than 1 (Figure 6b, Figure S7, Supporting Information) further indicates that the synergistic effect of MMC-DHA may be attributable to an elevation of intra-mitochondrial lipid peroxidation as an underlying mechanism of enhanced anticancer efficacy.<sup>[21]</sup>

The biodistribution and tumor accumulation of MMC-DHA-PLN were examined by whole body and ex vivo optical imaging using a near-infrared dye, 1,1'-diiodo-3,3',3'-tetramethylindotricarbocyanine iodide (DiR), labeled formulation. In orthotopic EMT6/AR1 breast tumor-bearing mice, fluorescence images acquired after i.v. injection of MMC-DHA-PLN (DiR) showed strong tumor accumulation and prolonged circulation and retention of MMC-DHA-PLN (Figure 6c,d), which was in contrast to free DiR dye that quickly diminished within 24 h (Figure S8, Supporting Information). In line with the in vitro cytotoxicity results, MMC-DHA-PLN treatment effectively inhibited tumor growth over a 30 d period and significantly prolonged the host survival compared to all other treatment groups (Figure 6e,f) and our previous DHA-free MMC-PLN system.<sup>[9a]</sup> Treatment with equivalent doses of free MMC-DHA induced severe myelosuppression as indicated by low platelet (PLT) and white blood cell (WBC) counts, whereas the treatment with MMC-DHA-PLN did not cause any noticeable change in body weight or reduction in blood cell counts (Figure 6g,h). This superior therapeutic outcome further confirmed the efficiency of controlled drug release of MMC-DHA-PLN (Figure 3g) to improve anticancer efficacy in MDR tumor without inducing unwanted adverse effects.

### 3. Conclusions

In summary, this work reports a novel “two-step” strategy to tackle multifaceted MDR using a composite nanoparticle system to first overcome membrane rigidity and then target mitochondria in MDR cancer cells. Spatial co-localization of DHA and MMC in the same PLN is critical to enhance cytoplasmic drug accumulation across the rigid membrane and to maximize their synergistic anticancer effect on damaging mitochondria via elevated lipid peroxidation. Coordination of cellular biophysical interactions between nanomaterial DHA and rigid membrane as well as intracellular bioreactions between DHA and the co-loaded anticancer prodrug MMC is crucial to enhance subcellular drug delivery and increase efficacy of chemotherapy. This work suggests a novel approach to orchestrating multiple functional components within a nano-carrier to overcome multifactorial MDR in cancer cells.

### 4. Experimental Section

**Characterization of PLN:** Particle size,  $\zeta$ -potential, and PDI of various PLN formulations were measured using a Zetasizer (Nano-ZS, Malvern, England). To determine the encapsulation efficiency and loading

percentage of MMC and DHA, 200  $\mu$ L of PLN was centrifuged for 5 min at  $14\,000 \times g$  (Microfuge 18 Centrifuge, Beckman Coulter, Canada) through a 0.05  $\mu$ m ultrafree filter (Merck Millipore Ltd, Germany). The filtrate containing MMC and DHA was assayed by spectrophotometry at 364 and 237 nm, respectively, using SpectraMax Plus 384 microplate reader (Molecular Devices LLC, USA).<sup>[23]</sup> To determine particle morphology, 5  $\mu$ L of MMC-DHA-PLN suspension was pipetted onto a TEM grid, and the air-dried TEM grid was directly observed under TEM (7000H, Hitachi, Japan). Stability of MMC-DHA-PLN was also determined at both storage and serum conditions. For storage stability, MMC-DHA-PLN emulsion was stored at 4 °C over 28 d, and its size,  $\zeta$ -potential and PDI were determined by the Zetasizer. The serum stability of MMC-DHA-PLN was studied by incubating MMC-DHA-PLN in 50% fetal bovine serum (FBS) (Gibco Cell Culture, Canada) and 50% phosphate buffered saline (PBS) at 37 °C over 24 h. The transmittance of MMC-DHA-PLN in serum over time was determined at 750 nm by UV-vis (Agilent, USA). The degree of PLN aggregation in serum as measured by size and turbidity changes was compared to time zero when MMC-DHA-PLN was added into 10% FBS.<sup>[29]</sup> To determine the release kinetics of MMC, 2 mL of MMC-DHA-PLN suspension or free MMC-DHA solution were encased in a dialysis tube with a 12 000 molecular weight cutoff (Spectrum Laboratories Inc., USA) and then incubated in 100 mL of  $\alpha$ -Minimum Essential Medium ( $\alpha$ -MEM) (Gibco Cell Culture, Canada) supplemented with 10% FBS at 37 °C. At various time points over 96 h, 0.1 mL of release medium outside the dialysis tube was withdrawn. MMC concentrations were determined spectrophotometrically at 364 nm (SpectraMax Plus 384 microplate reader). The release curve of free MMC solution served as a control to delineate that the prolonged drug release from the MMC-DHA-PLN was not due to the barrier of the dialysis membrane.<sup>[30]</sup>

**Maintenance of EMT6 Murine Breast Cancer Cells:** Both parent drug-sensitive EMT6/WT cells and paired MDR EMT6/AR1 cells overexpressing *P-gp* efflux transporters (provided by Dr. Ian Tannock from Ontario Cancer Institute, Canada) were grown as monolayers in a plastic tissue culture flask (Corning, Sigma-Aldrich, Canada) in  $\alpha$ -MEM supplemented with 10% FBS at 37 °C in a humidified incubator (NuAire DHD AutoFlow 5510, USA) with 5% CO<sub>2</sub> (Linde, Canada) atmosphere. MDR EMT6/AR1 cells were grown in the medium containing additional 1  $\mu$ g mL<sup>-1</sup> of doxorubicin (DOX) to maintain their drug resistance.

**AFM of Membrane Rigidity:** AFM can provide high-resolution topography studies of cancer cells for measurement of their biophysical properties under physiological conditions.<sup>[31]</sup> Both sensitive EMT6/WT and MDR EMT6/AR1 murine breast cancer cells were seeded at a density of  $0.8 \times 10^6$  cells per 60 mm diameter Petri dish (VWR, USA) and incubated at 37 °C for 24 h. Then, cells were treated under the following conditions: 5% sterile dextrose, free MMC, free DHA, free MMC-DHA, or MMC-DHA-PLN, at concentrations of  $24 \times 10^{-6}$  M of MMC and  $14 \times 10^{-6}$  M of DHA for 1 or 4 h at 37 °C. The treatment medium was removed and cancer cells were gently washed three times with pre-warmed  $\alpha$ -MEM without FBS. Then, the Petri dish was mounted onto an inverted optical microscope (Eclipse-Ti, Nikon Instrument Inc., USA). A 50 nm radius pyramidal tip (Veeco Instruments Inc., USA) was used to indent cancer cells. Indentation was applied via contact mode of AFM (Bioscope Catalyst, Bruker Corporation, USA) on the membrane of a single intact cell. The triggering force was set at 5 nN according to Costa and Yin.<sup>[32]</sup> Force measurements of each cell were repeated five times at the cell center (i.e., over the nucleus) to ensure no significant change of Young's modulus. The standard Hertz model is used in AFM to quantify mechanical properties of living cells by applying it to fit the rising slope of an approach curve before relaxation.<sup>[33]</sup> Young's modulus ( $E$ ), as a measure of the mechanical elasticity of the cell membrane was calculated from the indentation force applied on the cell membrane using Equation (1) provided by Nanoscope Analysis software (version 1.50, Bruker Corporation, USA)

$$F = \left(\frac{4}{3}\right) \times \sqrt{a} \times \left[\frac{E}{1-\nu^2}\right] \times h^{\frac{3}{2}} \quad (1)$$

where  $F$  is the loading force,  $a$  (50 nm) is the radius of the indenting tip,  $\nu$  (0.3) is the Poisson ratio of the cell,<sup>[34]</sup> and  $h$  is the indentation depth. Twenty cells per Petri dish were measured and measurements were completed within 20 min.

**Quantitation of Intracellular MMC Accumulation:** Both drug-sensitive EMT6/WT and MDR EMT6/AR1 cells were seeded at a density of  $0.8 \times 10^6$  cells per 60 mm diameter Petri dish (VWR) and allowed to grow at 37 °C for 24 h. Cells were then treated with free MMC, free MMC-DHA, MMC-PLN, or MMC-DHA-PLN at  $24 \times 10^{-6}$  M of MMC either alone or in combination with  $14 \times 10^{-6}$  M of DHA for 1 or 4 h. Then, the cells were washed with prewarmed PBS, trypsinized (Gibco Cell Culture) and collected into 1.5 mL centrifuge microtubes (Axygen, Corning, USA) followed by centrifugation at  $366 \times g$  at 4 °C for 5 min (Eppendorf 5702R, Eppendorf Corp. Canada). The supernatant was discarded and the cell pellet was lysed according to the protocol of Wong et al.<sup>[24]</sup> using 200  $\mu$ L of PBS containing 1% Triton X-100 detergent (Sigma-Aldrich, USA) followed by agitation on ice by a vortex mixer (Thermo Fisher Scientific, Canada) at speed "5" for 20 min. Homogenized cells were centrifuged at  $366 \times g$  at 4 °C for an additional 10 min, and the supernatant was analyzed at 364 nm using a SpectraMax PLUS384 microplate reader.<sup>[24]</sup>

**Fluorescence Microscopy of Intracellular PLN Localization:** Both EMT6/WT and EMT6/AR1 cells were seeded at a density of  $0.8 \times 10^6$  cells per 60 mm diameter Petri dish (VWR) in 3 mL of growth medium followed by 24 h incubation at 37 °C. Cancer cells were exposed to NR co-loaded PLN in different formulations: blank PLN (NR), MMC-PLN (NR), MMC-PLN (NR) + free DHA, MMC-DHA-PLN (NR), at final concentrations of  $105 \times 10^{-6}$  M of NR,  $24 \times 10^{-6}$  M of MMC, and  $14 \times 10^{-6}$  M of DHA for 4 h. Then, each Petri dish was gently washed three times with prewarmed PBS. Cell nuclei were stained with Hoescht 33342 (Molecular Probes, Life Technologies, USA) at  $0.5 \mu\text{g mL}^{-1}$  for 20 min at 37 °C followed by additional two times wash with prewarmed PBS. Both treated EMT6/WT and EMT6/AR1 cells were imaged under fluorescence microscopy (EVOS fl, AMG, USA) using the standard filter set of red fluorescent protein ( $\lambda_{\text{excitation}}/\lambda_{\text{emission}} = 488 \text{ nm}/593 \text{ nm}$ ) for NR and 4', 6-diamidino-2-phenylindole dihydrochloride ( $\lambda_{\text{excitation}}/\lambda_{\text{emission}} = 358 \text{ nm}/461 \text{ nm}$ ) for nuclei.

**Flow Cytometry Analysis of DHA Effect on Intracellular Uptake of PLN:** Both drug-sensitive EMT6/WT and drug-resistant EMT6/AR1 cells were seeded at a density of  $0.5 \times 10^6$  cells per 100 mm diameter Petri dish (VWR) in 3 mL of growth medium followed by 24 h incubation at 37 °C. Then, cancer cells were treated with 5% dextrose and three PLN formulations: MMC-PLN (NR), MMC-PLN (NR) + free DHA, and MMC-DHA-PLN (NR), at 4 and 37 °C for 4 h at final concentrations of  $105 \times 10^{-6}$  M of NR,  $24 \times 10^{-6}$  M of MMC, and  $14 \times 10^{-6}$  M of DHA for 4 h (the same final concentrations as previous fluorescent microscopy study). After the treatment, cells were fixed with 75% ethanol overnight and analyzed using a BD FACSCanto flow cytometer (BD Biosciences, USA). NR fluorescence was detected by tuning the laser at  $\lambda_{\text{excitation}} = 488 \text{ nm}$  and emission was collected using PE channel (filter 585/42 nm). Cancer cells treated with 5% dextrose (control) were used to detect any cellular autofluorescence. Ten thousand ( $1 \times 10^4$ ) events per sample were acquired and a nondamaged and uniform cell population gated and analyzed using FlowJo (FlowJo LLC, USA).

**TBARS Assay of Lipid Peroxidation:** The thiobarbituric acid reactive substance (TBARS) assay is based on the reactivity of an end product of lipid peroxidation, MDA with thiobarbituric acid (TBA) to form MDA-TBA adduct to determine the level of lipid peroxidation. To evaluate whether MMC-DHA-PLN elevated oxidative damage through lipid peroxidation, both sensitive EMT6/WT and resistant EMT6/AR1 cells were seeded in polystyrene 75 cm<sup>2</sup> flask (Corning, USA) at a density of  $2 \times 10^6$  cells per flask. After 24 h growth at 37 °C, the cells were treated with blank PLN, free MMC, free DHA, free MMC-DHA, or MMC-DHA-PLN at concentrations of  $24 \times 10^{-6}$  M of MMC and  $14 \times 10^{-6}$  M of DHA for 4 or 24 h. The TBARS assay was performed according to the protocol provided by the Lipid Peroxidation (MDA) Assay Kit (Abcam Inc., Canada).

**Confocal Microscopy Imaging of Lipid Peroxidation in Living Cells:** Both sensitive EMT6/WT and resistant EMT6/AR1 cells were seeded at

a density of  $0.3 \times 10^6$  per 35 mm diameter glass bottom culture dish (MatTek Corporation, USA) and allowed to grow in 3 mL of growth medium at 37 °C for 24 h. Cancer cells were treated with MMC-DHA-PLN at  $24 \times 10^{-6}$  M of MMC and  $14 \times 10^{-6}$  M of DHA for 4 h followed by three washes using prewarmed growth medium. Then,  $10 \times 10^{-6}$  M of Image-iT Lipid Peroxidation sensor (Molecular Probes, Life Technologies) and  $0.5 \mu\text{L mL}^{-1}$  Hoeschst 33342 nucleic acid dye (Molecular Probes, Life Technologies) were added to the cells followed by another 30 min incubation at 37 °C. Cells were then washed three times with prewarmed PBS and imaged at 354 nm (blue channel) for nuclei, 488 nm (green channel) for lipid peroxidation and 581 nm (red channel) for nonlipid peroxidation using a Zeiss LSM 510 laser scanning microscopy (Carl Zeiss Canada Ltd., Canada).

**Confocal Microscopy Co-Localization of Lipid Peroxidation and Mitochondria in Living Cells:** Both sensitive EMT6/WT and MDR EMT6/AR1 cells were seeded at a density of  $0.3 \times 10^6$  per 35 mm diameter glass bottom culture dish and allowed to grow in 3 mL of growth medium at 37 °C for 24 h. Cancer cells were then treated with either 5% dextrose or MMC-DHA-PLN at concentrations of  $24 \times 10^{-6}$  M MMC and  $14 \times 10^{-6}$  M DHA for 4 h followed by three-times washing with prewarmed growth medium. After treatments,  $10 \times 10^{-6}$  M of Image-iT Lipid Peroxidation sensor,  $200 \times 10^{-9}$  M of Mitotracker Deep Red FM (Molecular Probes, Life Technologies) and  $0.5 \mu\text{L mL}^{-1}$  Hoeschst 33342 nucleic acid dye (Molecular Probes, Life Technologies) were added to the cells followed by another 30 min incubation at 37 °C. Cells were washed three times with prewarmed PBS, and then imaged at 354 nm (Hoeschst33342 channel) for nuclei, 488 nm (FITC channel) for lipid peroxidation, and 644 nm (Alexa Fluor 647 channel) for Mitotracker Deep Red FM using a Zeiss LSM 510 laser scanning microscopy (Carl Zeiss Canada, Ltd.). The degree of co-localization between lipid peroxidation (green dye) and mitochondria (red dye) was quantitatively evaluated by PCC.

**TEM of Mitochondrial Morphological Damages:** EMT6/WT and EMT6/AR1 cells were seeded at a density of  $0.5 \times 10^6$  cells per well in a 6-well culture plate (Falcon, Thermal Fisher Scientific, Canada) and allowed to grow in 5 mL of growth medium at 37 °C for 24 h. Then, they were exposed to 5% dextrose (control) or MMC-DHA-PLN at concentrations of  $24 \times 10^{-6}$  M of MMC and  $14 \times 10^{-6}$  M of DHA for 4 or 24 h. The treatment medium was then removed and cells were washed three times with prewarmed PBS. For the TEM analysis of cancer cells, cells from control group (treated with 5% dextrose) and from MMC-DHA-PLN treated groups were chemically fixed in polystyrene treated culture plates with 4% paraformaldehyde and 1% glutaraldehyde in 0.1 M phosphate buffer at pH 7.2 for 1 h. The cells were then postfixed with 1% osmium tetroxide in 0.1 M phosphate buffer at pH 7.2 for 20 min. The fixed cells were then dehydrated in a graded gradient ethanol series and embedded in Epon618 (Canemco & Marivac, Canada). Ultrathin sections of embedded cancer cells were cut into 80–90 nm thickness and further stained with 5% uranyl acetate and 5% lead citrate for 10 min each. Finally, the stained sections were mounted onto TEM grids and were examined by Hitachi H7000 electron microscope using an accelerating voltage of 100 kV.

**MTT Cell Viability Assay for Mitochondrial Dysfunction:** MTT assay measures an ability of viable cancer cells to convert MTT into formazan using mitochondrial enzymes, and thus is considered as an indicator for determination of mitochondrial dysfunctions.<sup>[28]</sup> Both drug-sensitive EMT6/WT and MDR EMT6/AR1 cells were seeded at a density of  $5 \times 10^3$  cells per well in a 96-well plate (Corning, USA) for 24 h at 37 °C. The cells were treated with either free drug solution (free MMC, free DHA, free MMC-DHA) or nanoparticle formulations (blank PLN, MMC-PLN, DHA-PLN, and MMC-DHA-PLN) for an additional 24 h. All treatments were freshly prepared in growth medium based on MMC concentrations ranging from  $0.01 \times 10^{-6}$  to  $200 \times 10^{-6}$  M. Treatment with 5% dextrose was used as a negative control for all drug groups. MTT assay was performed according to the provided protocol (Sigma-Aldrich).

**Orthotopic Breast Tumor Murine Model:** All animal experiments were approved by the Animal Care Committee of University Health Network

at the Ontario Cancer Institute and conducted in accordance with the Canadian Council on Animal Care Guidelines. Eight-week old female Balb/c mice were purchased from Jackson Laboratory and housed at the Ontario Cancer Institute. MDR EMT6/WT breast tumors were grown orthotopically by injecting 30  $\mu\text{L}$  of  $1 \times 10^6$  MDR EMT6/AR1 cancer cells in growth medium into the right inguinal mammary fat pad of mouse. When tumor size reached  $\approx 100 \text{ mm}^3$ , the mice were randomly grouped into various treatments for biodistribution, efficacy and toxicity study.

**In Vivo Biodistribution of PLN:** The biodistribution of MMC-DHA-PLN was examined by in vivo whole body and ex vivo organ fluorescence imaging using co-loaded DiR (Molecular Probes, Life Technologies) as a fluorophore. MMC-DHA-PLN (DiR) or free DiR at dose of  $0.5 \text{ mg kg}^{-1}$  of DiR was injected i.v. via the tail vein of MDR tumor-bearing mice. At various time points up to 9 d, mice were anaesthetized with 2% isoflurane via nose cones and in vivo whole body images were acquired using a Xenogen IVIS Spectrum (Caliper Life Sciences Inc., USA) imager at  $\lambda_{\text{ex}}/\lambda_{\text{em}} = 745 \text{ nm}/840 \text{ nm}$ , respectively. For ex vivo imaging, the major organ (heart, lungs, liver, spleen, intestine, and kidneys) and breast tumor were perfused using ice-cold saline via the left ventricle, then dissected and imaged.

**Efficacy and Toxicity Evaluation of MMC-DHA-PLN:** Treatments were initiated once breast tumor reached around  $100 \text{ mm}^3$ . The treatments comprised groups of mice receiving i.v. injections of 5% dextrose, blank PLN, free MMC-DHA, MMC-PLN + free DHA, or MMC-DHA-PLN with each treatment being administered on day 0 and day 5 at MMC dose level 4.00 and  $2.36 \text{ mg kg}^{-1}$  of DHA (1:0.6 molar ratio). Tumor volume and body weights of all mice were measured every other day. Mice were euthanized either when there was 20% weight loss or when tumor volume reached  $500 \text{ mm}^3$ , in accordance with Animal Care Committee Guidelines. Tumor volume growth was calculated according to  $(\text{Length} \times \text{Width}^2)/2$ . Additionally, to determine any MMC-induced myelosuppression, whole blood was collected from the saphenous vein at the animal's end point into ethylenediaminetetraacetic acid coated tubes and immediately analyzed using Hemavet 950FS (Drew Scientific Inc., USA) to determine the number of platelets and white blood cells of various treatment groups.

**Statistical Analysis:** Student's *t*-test was used for comparisons between two groups, and one-way analysis of variance (ANOVA) followed by postdoc Tukey's test was used for multiple comparisons using GraphPad Prism 6.0 (GraphPad Software Inc., USA) with *p* value less than 0.05 indicating statistical significance. Quantifying co-localization using PCC was performed by WCIF Image J for microscopy.

## Supporting Information

Supporting information is available from the Wiley Online Library or from the author.

## Acknowledgements

R.X.Z. and L.Y.L. contributed equally to this work. The authors gratefully acknowledge the Canadian Breast Cancer Foundation (CBCF)-Ontario Region for funding this project; Natural Sciences and Engineering Research Council of Canada for the equipment grants; University open scholarships to R.X.Z. and J.L.; Canada Research Chair in Micro and Nano Engineering Systems to Y.S.; W. Jun from Department of Mechanical and Industrial Engineering for AFM setup; Dr. Shana O. Kelley for usage of flow cytometer and software FlowJo.

## Conflict of Interest

The authors declare no conflict of interest.

## Keywords

coordinating biointeraction and bioreaction, multidrug-resistant cancer cells, nanocarrier materials, overcoming membrane rigidity, targeting mitochondria

Received: February 13, 2017

Revised: March 22, 2017

Published online:

- [1] a) C. Holohan, S. Van Schaeybroeck, D. B. Longley, P. G. Johnston, *Nat. Rev. Cancer* **2013**, *13*, 714; b) G. Housman, S. Byler, S. Heerboth, K. Lapinska, M. Longacre, N. Snyder, S. Sarkar, *Cancers* **2014**, *6*, 1769.
- [2] a) M. M. Gottesman, T. Fojo, S. E. Bates, *Nat. Rev. Cancer* **2002**, *2*, 48; b) H. L. Wong, X. Y. Wu, R. Bendayan, in *Pharmaceutical Perspectives of Cancer Therapeutics* (Eds: Y. Lu, R. I. Mahato), Springer Science + Business Media LLC, New York **2009**, pp. 121–148; c) C. Peetla, S. Vijayaraghavalu, V. Labhasetwar, *Adv. Drug Delivery Rev.* **2013**, *65*, 1686.
- [3] a) S. Fulda, L. Galluzzi, G. Kroemer, *Nat. Rev. Drug Discovery* **2010**, *9*, 447; b) S. S. Sabharwal, P. T. Schumacker, *Nat. Rev. Cancer* **2014**, *14*, 709; c) L. Milane, M. Trivedi, A. Singh, M. Talekar, M. Amiji, *J. Controlled Release* **2015**, *207*, 40; d) A. Chatterjee, E. Mambo, D. Sidransky, *Oncogene* **2006**, *25*, 4663; e) E. Roundhill, D. Turnbull, S. Burchill, *FASEB J.* **2016**, *30*, 1712.
- [4] A. Jhaveri, V. Torchilin, *Expert Opin. Drug Delivery* **2016**, *13*, 49.
- [5] R. X. Zhang, T. Ahmed, L. Y. Li, J. Li, A. Z. Abbasi, X. Y. Wu, *Nanoscale* **2017**, *9*, 1334.
- [6] S. Kunjachan, A. Blauz, D. Mockel, B. Theek, F. Kiessling, T. Etrych, K. Ulbrich, L. van Bloois, G. Storm, G. Bartosz, B. Rychlik, T. Lammers, *Eur. J. Pharm. Sci.* **2012**, *45*, 421.
- [7] a) Z. Binkhathlan, A. Lavasanifar, *Curr. Cancer Drug Targets* **2013**, *13*, 326; b) H. M. Coley, *Methods Mol. Biol.* **2010**, *596*, 341; c) G. Szakacs, J. K. Paterson, J. A. Ludwig, C. Booth-Genthe, M. M. Gottesman, *Nat. Rev. Drug Discovery* **2006**, *5*, 219.
- [8] a) R. X. Zhang, H. L. Wong, H. Y. Xue, J. Y. Eoh, X. Y. Wu, *J. Controlled Release* **2016**, *240*, 489; b) R. X. Zhang, P. Cai, T. Zhang, K. Chen, J. Li, J. Cheng, K. S. Pang, H. A. Adissu, A. M. Rauth, X. Y. Wu, *Nanomedicine* **2016**, *12*, 1279; c) H. L. Wong, R. Bendayan, A. M. Rauth, Y. Li, X. Y. Wu, *Adv. Drug Delivery Rev.* **2007**, *59*, 491; d) P. Prasad, J. Cheng, A. Shuhendler, A. M. Rauth, X. Y. Wu, *Drug Delivery Transl. Res.* **2012**, *2*, 95; e) K. A. Whitehead, R. Langer, D. G. Anderson, *Nat. Rev. Drug Discovery* **2009**, *8*, 129.
- [9] a) A. J. Shuhendler, P. Prasad, R. X. Zhang, M. A. Amini, M. Sun, P. P. Liu, R. G. Bristow, A. M. Rauth, X. Y. Wu, *Mol. Pharmaceutics* **2014**, *11*, 2659; b) C. Peetla, R. Bhave, S. Vijayaraghavalu, A. Stine, E. Kooijman, V. Labhasetwar, *Mol. Pharmaceutics* **2010**, *7*, 2334; c) T. Takahashi, T. Furuchi, A. Naganuma, *Cancer Res.* **2006**, *66*, 11932; d) S. S. Chauhan, X. J. Liang, A. W. Su, A. Pai-Panandiker, D. W. Shen, J. A. Hanover, M. M. Gottesman, *Br. J. Cancer* **2003**, *88*, 1327.
- [10] a) J. Cheng, Q. Liu, A. J. Shuhendler, A. M. Rauth, X. Y. Wu, *Colloids Surf., B* **2015**, *130*, 164; b) Q. Liu, A. Shuhendler, J. Cheng, A. M. Rauth, P. O'Brien, X. Y. Wu, *Breast Cancer Res. Treat.* **2010**, *121*, 323.
- [11] a) Z. Liu, R. Bendayan, X. Y. Wu, *J. Pharm. Pharmacol.* **2001**, *53*, 779; b) D. Y. Alakhova, A. V. Kabanov, *Mol. Pharmaceutics* **2014**, *11*, 2566.
- [12] a) Y. Barenholz, *Subcell. Biochem.* **2004**, *37*, 167; b) J. W. Hinrichs, K. Klappe, M. van Riesen, J. W. Kok, *J. Lipid Res.* **2005**, *46*, 2367; c) C. Aleman, J. P. Annereau, X. J. Liang, C. O. Cardarelli, B. Taylor, J. J. Yin, A. Aszalos, M. M. Gottesman, *Cancer Res.* **2003**, *63*, 3084.

- [13] a) C. Peetla, S. Jin, J. Weimer, A. Elegbede, V. Labhasetwar, *Langmuir* **2014**, *30*, 7522; b) S. Vijayaraghavalu, C. Peetla, S. Lu, V. Labhasetwar, *Mol. Pharmaceutics* **2012**, *9*, 2730; c) V. Raghavan, S. Vijayaraghavalu, C. Peetla, M. Yamada, M. Morisada, V. Labhasetwar, *Langmuir* **2015**, *31*, 11564.
- [14] a) S. V. Mussi, R. C. Silva, M. C. Oliveira, C. M. Lucci, R. B. Azevedo, L. A. Ferreira, *Eur. J. Pharm. Sci.* **2013**, *48*, 282; b) A. Beloqui, M. Á. Solinís, A. Rodríguez-Gascón, A. J. Almeida, V. Prát, *Nanomedicine* **2016**, *12*, 143.
- [15] a) W. Stillwell, S. R. Wassall, *Chem. Phys. Lipids* **2003**, *126*, 1; b) M. Pinot, S. Vanni, S. Pagnotta, S. Lacas-Gervais, L. A. Payet, T. Ferreira, R. Gautier, B. Goud, B. Antonny, H. Barelli, *Science* **2014**, *345*, 693.
- [16] N. Merendino, L. Costantini, L. Manzi, R. Molinari, D. D'Eliseo, F. Velotti, *Biomed. Res. Int.* **2013**, *2013*, 310186.
- [17] a) M. M. Paz, C. A. Pritsos, in *Advances in Molecular Toxicology*, Vol. 6 (Ed: J. C. Fishbein), Elsevier B.V., Amsterdam, Netherlands **2012**, pp. 243–299; b) A. M. Rauth, T. Melo, V. Misra, *Int. J. Radiat. Oncol., Biol., Phys.* **1998**, *42*, 755.
- [18] X. Y. Wu, *Expert Opin. Drug Delivery* **2016**, *13*, 609.
- [19] S. Selvamuthukumar, R. Velmurugan, *Lipids Health Dis.* **2012**, *11*, 159.
- [20] a) Y. Li, N. Taulier, A. M. Rauth, X. Y. Wu, *Pharm. Res.* **2006**, *23*, 1877; b) H. L. Wong, R. Bendayan, A. M. Rauth, X. Y. Wu, *J. Controlled Release* **2006**, *116*, 275; c) H. L. Wong, A. M. Rauth, R. Bendayan, J. L. Manias, M. Ramaswamy, Z. Liu, S. Z. Erhan, X. Y. Wu, *Pharm. Res.* **2006**, *23*, 1574.
- [21] T. C. Chou, *Cancer Res.* **2010**, *70*, 440.
- [22] a) J. A. Menendez, M. del Mar Barbacid, S. Montero, E. Sevilla, E. Escrich, M. Solanas, H. Cortes-Funes, R. Colomer, *Eur. J. Cancer* **2001**, *37*, 402; b) J. A. Menendez, R. Lupu, R. Colomer, *Eur. J. Cancer Prev.* **2005**, *14*, 263.
- [23] A. J. Shuhendler, R. Y. Cheung, J. Manias, A. Connor, A. M. Rauth, X. Y. Wu, *Breast Cancer Res. Treat.* **2010**, *119*, 255.
- [24] H. L. Wong, R. Bendayan, A. M. Rauth, H. Y. Xue, K. Babakhanian, X. Y. Wu, *J. Pharmacol. Exp. Ther.* **2006**, *317*, 1372.
- [25] a) E. Blanco, H. Shen, M. Ferrari, *Nat. Biotechnol.* **2015**, *33*, 941; b) E. Frohlich, *Int. J. Nanomed.* **2012**, *7*, 5577.
- [26] S. Zhang, H. Gao, G. Bao, *ACS Nano* **2015**, *9*, 8655.
- [27] K. W. Dunn, M. M. Kamocka, J. H. McDonald, *Am. J. Physiol.: Cell Physiol.* **2011**, *300*, C723.
- [28] M. D. Brand, D. G. Nicholls, *Biochem. J.* **2011**, *435*, 297.
- [29] N. Maeda, Y. Takeuchi, M. Takada, Y. Sadzuka, Y. Namba, N. Oku, *J. Controlled Release* **2004**, *100*, 41.
- [30] Y. Zhou, C. He, K. Chen, J. Ni, Y. Cai, X. Guo, X. Y. Wu, *J. Controlled Release* **2016**, *243*, 11.
- [31] a) H. Liu, Q. Tan, W. R. Geddie, M. A. Jewett, N. Phillips, D. Ke, C. A. Simmons, Y. Sun, *Cell Biochem. Biophys.* **2014**, *68*, 241; b) H. Liu, J. Wen, Y. Xiao, J. Liu, S. Hopyan, M. Radisic, C. A. Simmons, Y. Sun, *ACS Nano* **2014**, *8*, 3821.
- [32] K. D. Costa, F. C. Yin, *J. Biomech. Eng.* **1999**, *121*, 462.
- [33] J. L. Alonso, W. H. Goldmann, *Life Sci.* **2003**, *72*, 2553.
- [34] W. R. Trickey, F. P. Baaijens, T. A. Laursen, L. G. Alexopoulos, F. Guilak, *J. Biomech.* **2006**, *39*, 78.